

Temperature-Dependent Effects of Alkyl Substitution on Diarylamine Antioxidant Reactivity

Ron Shah, Jia-Fei Poon, Evan A. Haidasz, and Derek A. Pratt*

Cite This: *J. Org. Chem.* 2021, 86, 6538–6550

Read Online

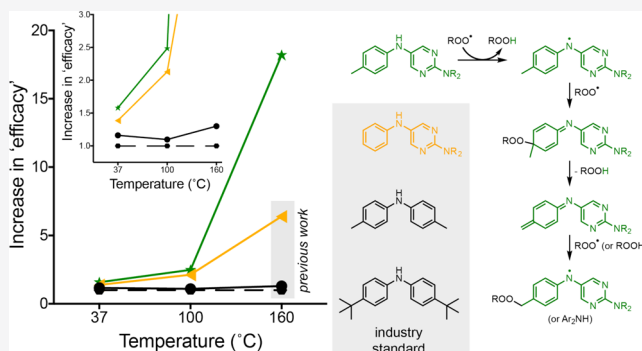
ACCESS |

Metrics & More

Article Recommendations

Supporting Information

ABSTRACT: Alkylated diphenylamines are among the most efficacious radical-trapping antioxidants (RTAs) for applications at elevated temperatures since they are able to trap multiple radical equivalents due to catalytic cycles involving persistent diphenylnitroxide and diphenylaminyl radical intermediates. We have previously shown that some heterocyclic diarylamine RTAs possess markedly greater efficacy than typical alkylated diphenylamines, and herein, report on our efforts to identify optimal alkyl substitution of the scaffold, which we had found to be the ideal compromise between reactivity and stability. Interestingly, the structure–activity relationships differ dramatically with temperature: *para*-alkyl substitution slightly increased reactivity and stoichiometry at 37 and 100 °C due to more favorable (stereo)electronic effects and corresponding diarylaminyll/diarylnitroxide formation, while *ortho*-alkyl substitution slightly decreased both reactivity and stoichiometry. No such trends were evident at 160 °C; instead, the compounds were segregated into two groups based on the presence/absence of benzylic C–H bonds. Electron spin resonance spectroscopy indicates that increased efficacy was associated with lesser diarylnitroxide formation, and deuterium-labeling suggests that this is due to abstraction of the benzylic H atom, precluding nitroxide formation. Computations predict that this reaction path is competitive with established fates of the diarylaminyll radical, thereby minimizing the formation of off-cycle products and leading to significant gains in high-temperature RTA efficacy.



INTRODUCTION

Autoxidation, the archetype free-radical chain reaction, is responsible for the degradation of virtually all hydrocarbon-based materials including rubber, lubricants, plastics, and biological membranes (Figure 1A).^{1,2} The key propagation steps comprise the addition of O₂ to a substrate-derived carbon-centered radical to form a peroxy radical and the subsequent abstraction of a H-atom from the hydrocarbon substrate. The chain reaction can be initiated in a variety of ways, but arguably the most relevant are either thermolysis of hydroperoxides or their heterolysis by dissociative electron transfer from low-valent metal atoms or other reductants to give hydroxyl and/or alkoxy radicals. Radical-trapping antioxidants (RTAs) such as hindered phenols (e.g., butylated hydroxytoluene, BHT) and diarylamines (e.g., alkylated diphenylamines, **1**) inhibit autoxidation by a reaction with chain-carrying peroxy radicals by H-atom transfer (HAT).^{3,4}

Phenols, such as BHT, generally trap two peroxy radicals since the phenoxyl radical formed from HAT can combine with a second peroxy radical (Figure 1B).^{3,4} However, at elevated temperatures (i.e., to which lubricating oils are subjected in internal combustion engines, and polymers processed by extrusion), BHT and other phenols trap fewer than one radical because the peroxidic adduct decomposes to

yield chain-initiating or chain-propagating radicals.⁵ In contrast, the aminyl radical derived from an alkylated diphenylamine can undergo formal oxygen-atom transfer (OAT) from a peroxy radical to yield a nitroxide (Figure 1C, red).^{6,7} Nitroxide formation enables the trapping of many more radicals. Nitroxides undergo rapid reactions with alkyl radicals to yield alkoxyamines (Figure 1C, blue), from which **1** can reform either by N–O homolysis and in-cage disproportionation⁸ or a retro-carbonyl-ene reaction and tautomerization (Figure 1D).⁹ Alternatively, nitroxides catalyze the cross-dismutation of alkylperoxy and hydroperoxy radicals (Figure 1E).^{10,11} The former pathway requires elevated temperatures to surmount the barrier for N–O cleavage (>120 °C), whereas the latter can occur at any temperature, provided sufficient hydroperoxy is formed in situ.^{12,13}

Received: February 14, 2021

Published: April 26, 2021



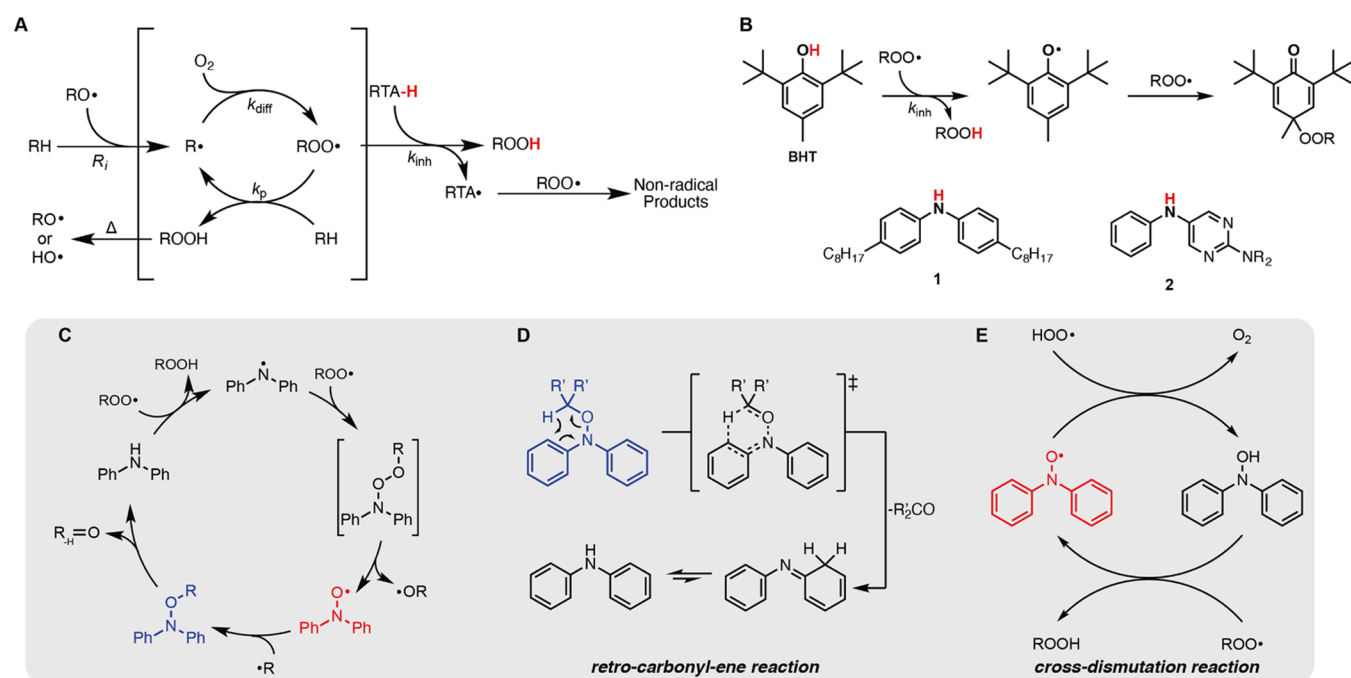
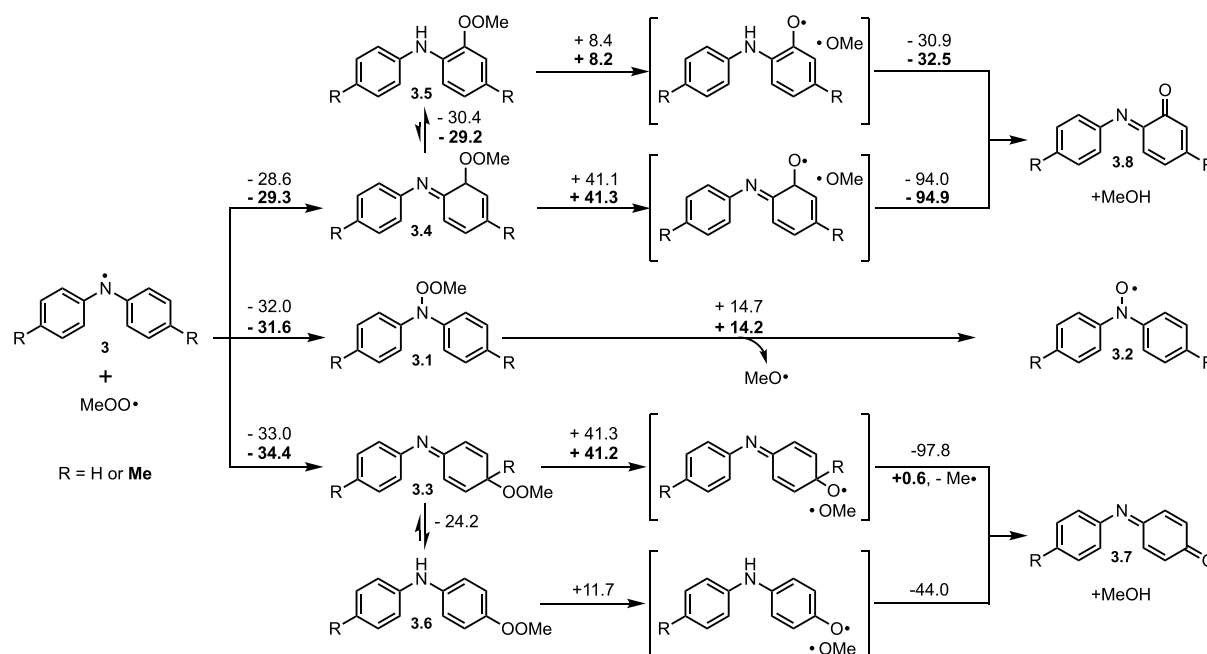


Figure 1. (A) Simplified mechanism of hydrocarbon autoxidation and its inhibition by a radical-trapping antioxidant (RTA). (B) Representative hindered phenol (butylated hydroxytoluene, BHT) and diarylamine RTAs. (C) Korcek's mechanism of catalytic radical trapping by diarylamine RTAs. (D) Retro-carbonyl-ene (RCE) reaction for the regeneration of diarylamines from their corresponding alkoxyamines. (E) Diarylnitroxide-catalyzed cross-dismutation of hydroperoxyl and alkylperoxyl radicals.

Scheme 1. CBS-QB3-Computed Thermochemistry (Enthalpies at 298 K in kcal/mol) for Competing Reactions of Diphenylaminyl and Ditolylaminyl Radicals with (Methyl)peroxyl Radicals



Alkyl substitution of diphenylamine, particularly in the *para* positions of the phenyl rings, increases its RTA activity. Alkyl groups stabilize the inherently electron-poor diphenylaminyl radical resulting from HAT¹³ and the diphenylnitroxide radical resulting from the subsequent OAT. However, perhaps more importantly, alkyl substitution increases the persistence of the diphenylaminyl radical and diphenylnitroxide, enabling them to engage in the reactions shown in Figure 1C,D. Indeed, commercial diphenylamine RTAs invariably possess alkyl

substitution on each aryl ring, although it is often implied that this is merely to increase solubility in hydrocarbons and minimize volatility for high-temperature applications.

We previously demonstrated that incorporation of nitrogen atoms in the aryl rings of diphenylamines combined with judicious selection of ring substituents results in air-stable compounds which are up to 200 times more reactive than di-*n*-octyldiphenylamine (1), an *n*-alkylated analogue of the prototypical industry standard, at ambient temperatures.^{14–17}

Scheme 2. CBS-QB3-Computed Thermochemistry (Enthalpies at 298 K in kcal/mol) for Competing Reactions of the Aminyl Radical Derived from 2 with (Methyl)peroxyl Radicals

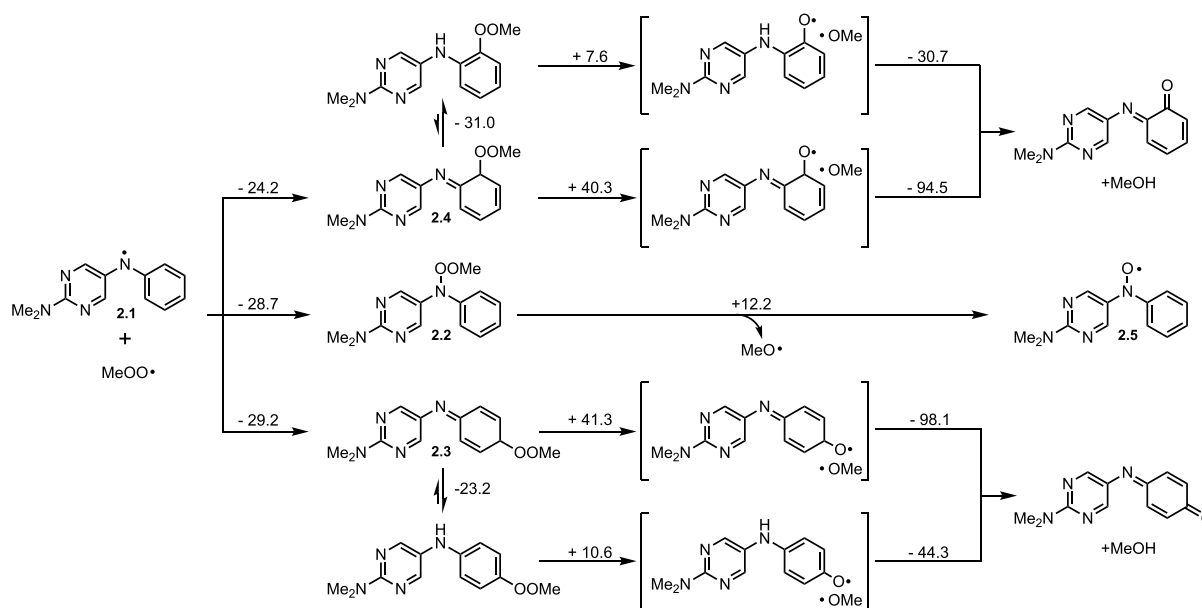
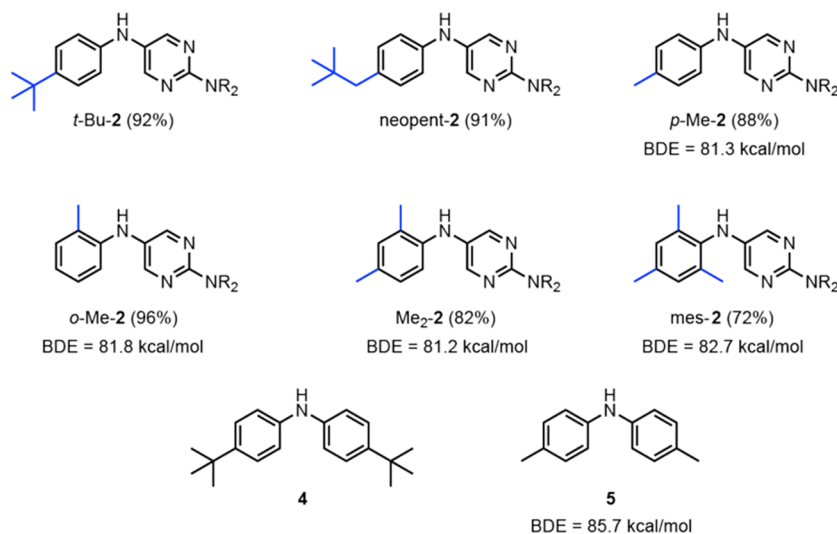


Chart 1. Diarylamines Studied in this Work and Corresponding BDEs Calculated for Select Examples using CBS-QB3



Following up on these preliminary results, we explored the reactivity of these compounds at elevated temperatures (160 °C) to find unprecedented inhibition of autoxidation relative to **1** by many examples.¹⁸ The most potent RTA under these conditions was *N*-phenylpyrimidine-2,5-diamine **2**, which was found to have a good balance of reactivity and stability to O₂/ROOH. Herein, we build on this result and explore the RTA activity of alkylated derivatives of **2**. This systematic study has enabled further improvement of **2** and sheds new light on the role of alkyl substitution on diarylamine RTAs, in general.

RESULTS

Computational Studies on Potential Fates of the Radicals Derived from Diarylamines. In earlier work, we used quantum chemical calculations to probe the extent to which nitroxide formation was preferred over peroxy radical addition to the aromatic rings of the diphenylaminyl radical (3).⁹ CBS-QB3 calculations suggested that addition of peroxy

radicals to the *para* position relative to the aminyl nitrogen is preferred by ~1 kcal/mol over formation of the peroxyamine precursor (3.1) to diphenylnitroxide (3.2, Scheme 1). In the peroxyamine intermediate (3.1), the O–O bond is much weaker than the N–O bond (14.7 vs 32.0 kcal/mol), cleaving to yield the nitroxide (3.2) and alkoxy radical, whereas in the *para*-coupled adduct (3.3), the C–O bond is much weaker than the O–O bond (33.0 vs 41.3 kcal/mol). Similarly, the *ortho*-adduct (3.4) also has a weaker C–O bond compared to the O–O bond (28.6 vs 41.1 kcal/mol), suggesting that at elevated temperatures, peroxy radical addition to the *ortho* and *para* positions is reversible and the intermediate diphenylaminyl radical (3) is funneled toward the nitroxide (3.2).

Following up on these calculations, we consider here the impact of including alkyl groups on the diphenylaminyl radical (data also shown in Scheme 1). Interestingly, we have found that peroxy radical addition to a ring carbon is predicted to be more favorable when the ring carbon bears an alkyl group (a

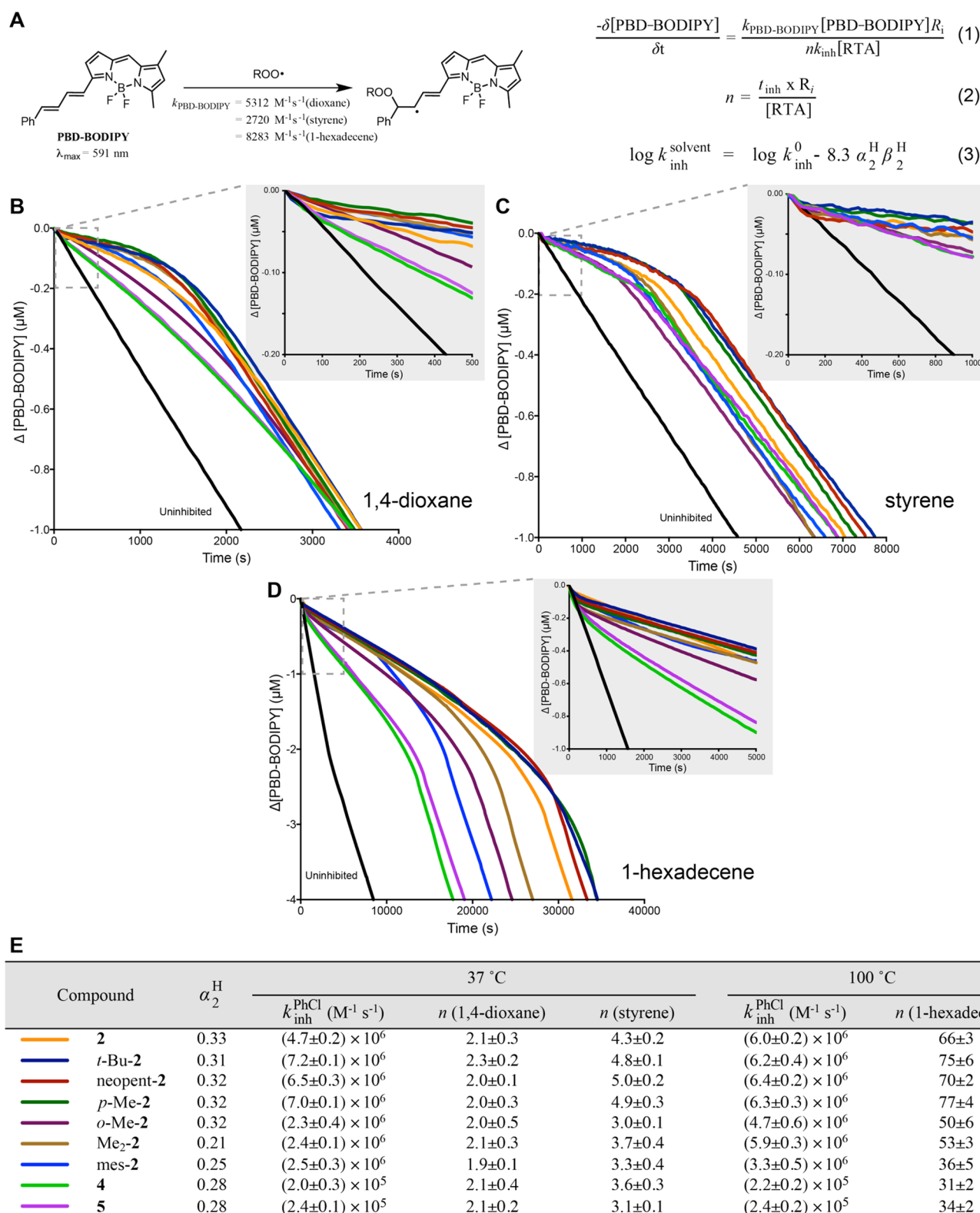


Figure 2. (A) PBD-BODIPY is used as the signal carrier in autoxidations of 1,4-dioxane and styrene at 37 °C and 1-hexadecene at 100 °C, enabling determination of inhibition rate constants (k_{inh} , eq 1) and stoichiometries (n , eq 2) for reactions of RTAs with chain-carrying peroxy radicals. (B) Representative data from co-oxidations of 1,4-dioxane (2.9 M) and PBD-BODIPY (10 μM) initiated by AIBN (6 mM) in PhCl at 37 °C monitored at 587 nm ($\epsilon = 123\,023 \text{ M}^{-1} \text{ cm}^{-1}$), (C) styrene (4.3 M) and PBD-BODIPY (10 μM) initiated by AIBN (6 mM) in PhCl at 37 °C monitored at 591 nm ($\epsilon = 139\,000 \text{ M}^{-1} \text{ cm}^{-1}$), and (D) 1-hexadecene (2.8 M) and PBD-BODIPY (10 μM) initiated by dicumyl peroxide (1 mM) in PhCl at 100 °C, monitored at 587 nm ($\epsilon = 131\,972 \text{ M}^{-1} \text{ cm}^{-1}$) inhibited by the various diarylamines. (E) Kinetic data derived for the diarylamines; data were corrected for H-bonding to 1,4-dioxane using the α_2^{H} values determined for the diarylamines and eq 3 (see the Supporting Information for data and details).

methyl group chosen for computational expediency). Thus, it would appear that alkylation must disfavor a follow-up reaction rather than initial ring addition. Given that the O–O BDEs in the adducts are roughly the same between the unalkylated and alkylated diphenylamine adducts (~41 kcal/mol), we must conclude that alkylation prevents tautomerization of the adduct to an arylperoxide (3.5, 3.6), which features a much weaker O–O bond. The resultant radicals may then undergo either in-cage disproportionation to yield observed imino quinones (3.7, 3.8),^{19,20} or participate in other reactions. Indeed, the tautomerization reaction is highly thermodynamically favorable (–30.4 and –24.2 kcal/mol for the *ortho*- and *para*-adducts, 3.4 and 3.3, respectively) and likely to be competitive with the highly endothermic reverse reactions (+28.6 and +33.0 kcal/mol for the *ortho*- and *para*-adducts, respectively). Introduction of the methyl group in the *para* position prevents the key tautomerization step, forcing the choice between C–O (BDE = 34.4 kcal/mol) and O–O (BDE = 41.2 kcal/mol) homolysis. Thus, it would appear that alkylation helps to funnel the diphenylaminyl radical toward nitroxide formation at elevated temperatures by suppressing tautomerization of the peroxy-diarylaminy radical.

Analogous computations were subsequently carried out on the diarylaminy radical derived from 2, which revealed a similar preference (Scheme 2). Formation of each of the peroxy adducts 2.2–2.4 was ~4 kcal/mol less favorable than for diphenylamine (Scheme 1), owing to the increased stability of the aminyl radical 2.1 (the N–H BDE in 2 is 81.8 kcal/mol, whereas those in diphenylamine and ditolylamine are 86.4 and 85.2 kcal/mol,⁹ respectively). As such, formation of the *para*-adduct (2.3) is still predicted to be favored slightly over the peroxyamine (2.2), which leads to the nitroxide (2.5). Moreover, ring addition followed by tautomerization remained a favorable pathway, which would preclude nitroxide formation. It should be pointed out that these calculations were carried out in the gas phase and that the kinetics of the processes have not been considered.

Compound Selection and Synthesis. Compounds in Chart 1 were selected to probe the effect of alkyl substitution on the reactivity of 2. Methyl substitution was considered in both the *ortho* and *para* positions, alone and in combination (*p*-Me-2, *o*-Me-2, Me₂-2, and mes-2). Bulky groups (*t*-butyl and neopentyl) were restricted to the *para* position (*t*-Bu-2 and neopent-2) since their inclusion in the *ortho* position(s) was expected to be highly detrimental. CBS-QB3 calculations reveal a small electronic effect of a methyl group when installed in the *para* position, as the N–H BDE drops from 81.8 kcal/mol in 2 to 81.3 in *p*-Me-2, which is erased when in the *ortho* position. This presumably arises due to the perturbation of electron delocalization in both the parent amine and the aminyl radical; the dihedral angle between the aryl rings increases from 55.2 to 57.5° in the former and 42.7 to 44.4° in the latter. However, introduction of a second methyl group in the *ortho* position induces a greater perturbation (to 64.3° in the amine and 58.1° in the radical), more than offsetting the electronic effects of the methyl groups on the aminyl radical and leading to an increased N–H BDE of 82.7 kcal/mol. These relatively small changes in BDE suggest that the inherent reactivity of the amines to peroxy radicals should be similar. Representative BDEs are included in Chart 1 and the computed structures of all diarylamines and corresponding aminyl radicals are included in the Supporting Information (SI).

The diarylamines were prepared by Buchwald–Hartwig cross-coupling of the appropriately alkylated aniline and *N,N*-dialkylamino-substituted pyrimidyl bromide (R = hexyl or octyl).^{15,18} The latter compounds were obtained from bromination and alkylation of 2-aminopyrimidine. In contrast with our previous work, wherein we have carried out analogous cross-couplings with Pd₂(dba)₃ and XPhos, we have since identified that BippyPhos is a better (and more economical) choice. This procedure was easily scalable, allowing us to obtain multigram quantities (>10 g) of our compounds in excellent yields. Diphenylamines 4 and 5, models of the industrial standard with either *n*- or *t*-alkyl substitution, were included in our studies for comparison and were synthesized using the same methodology.

Inhibited Autoxidations at 37 °C. The effect of alkyl substitution on the reactivity of 2 toward peroxy radicals was assessed by inhibited co-autoxidations of either 1,4-dioxane²¹ or styrene and PBD-BODIPY in chlorobenzene (Figure 2A).²² PBD-BODIPY, which is present in a trace amount (10 μM), serves simply as a signal carrier such that reaction progress can be monitored directly by conventional spectrophotometry. Using this approach, k_{inh} (the rate constant for H-atom transfer from the RTA to the peroxy radical) can be derived from the initial rate of the inhibited autoxidation (eq 1) and the number of radicals trapped per molecule of RTA (n) can be derived from the length of the inhibited period (eq 2). Representative data are shown in Figure 2B,C and the corresponding values of k_{inh} and n are given in the table in Figure 2E.

To provide insight on the inherent H-atom transfer reactivity of these compounds, the kinetic data determined from the dioxane co-autoxidations were corrected for the attenuation in reactivity of the amines due to hydrogen bonding to 1,4-dioxane.^{23,24} This kinetic solvent effect (KSE) is well established and can be accounted for using the Ingold–Abraham equation (eq 3),²³ wherein the α_2^H and β_2^H parameters represent the hydrogen bond-donating ability of the RTA and the hydrogen bond-accepting ability of the solvent, respectively.^{25,26} The α_2^H values of each of the compounds were measured using ¹H NMR and used to estimate rate constants in the absence of 1,4-dioxane (see SI for the data and the details).²⁷

Overall, the reactivities of the heterocyclic diarylamines were similar, with rate constants varying only ~threefold in the range from 2.3×10^6 to 7.2×10^6 M⁻¹ s⁻¹, consistent with the small differences in the computed N–H BDEs. All were expectedly more reactive than the models of the industrial standard 4 and 5.¹⁶ The stoichiometric values for the compounds varied as a function of the substrate: $n \sim 2$ in the 1,4-dioxane co-autoxidations and $n = 3–5$ in the styrene co-autoxidations. Derivatives lacking *ortho* substituents were at the upper end of the range while those with them were at the lower end.

Inhibited Autoxidations at 100 °C. With the foregoing baseline of reactivity established, we sought to determine the reactivity of the compounds under conditions that more closely approximate those in which diarylamines RTAs are used. We initially selected 100 °C for study as this is the maximum temperature at which we can acquire reliable, highly reproducible quantitative data (i.e., k_{inh} and n) using the PBD-BODIPY co-autoxidation approach. Representative data, obtained from co-autoxidations with 1-hexadecene, are presented in Figure 2D alongside values of k_{inh} and n derived therefrom. Most of the rate constants measured for the

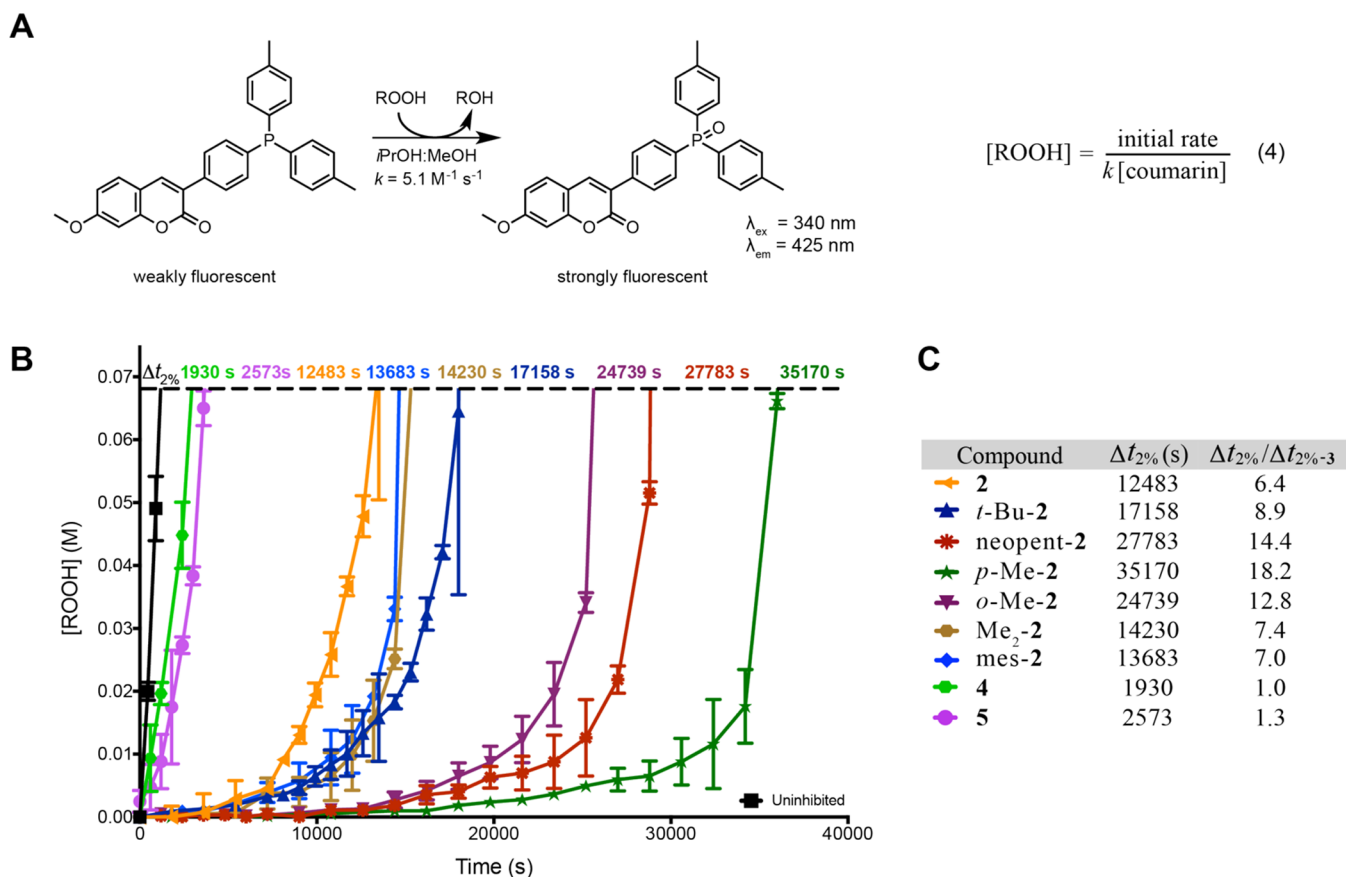


Figure 3. (A) Coumarin-conjugated triarylphosphine enables the quantification of hydroperoxides in *n*-hexadecane autoxidations using eq 4. (B) Hydroperoxide formation during the inhibited autoxidation of *n*-hexadecane at 160 °C. All autoxidations were carried out in a stirred-flow reactor under 2 L/min O₂ in the presence of 2 mM Primene-81R. (C) Absolute and relative inhibited periods (defined by the times at which reaction progress had reached 2% of the starting substrate concentration converted to hydroperoxide) of the various diarylamine RTAs.

compounds at 100 °C were similar to those obtained at 37 °C, which was expected on the basis of the small activation enthalpies for the reactions of diarylamines and peroxy radicals (e.g., $\log A = 6.9$ and $E_a = 2.5$ kcal/mol for 5).¹⁶ However, the reaction stoichiometries at 100 °C were much larger than those at 37 °C, which enabled a greater resolution of their radical-trapping capacities. Notably, all *para*-substituted compounds had greater stoichiometries compared to the *ortho*-substituted analogues, e.g., $n = 77$ for *p*-Me-2 vs $n = 36$ for mes-2.

Inhibited Autoxidations at 160 °C. The diarylamines were next investigated for their ability to inhibit the oxidation of a saturated hydrocarbon (*n*-hexadecane) upon heating to 160 °C in a stirred-flow reactor (2 mL/min O₂)—necessary to ensure that mass transfer of O₂ does not become rate-limiting.^{28,29} Primene (a tertiary alkylamine) was added to neutralize acids that are formed in the autoxidation as they are known to deactivate heterocyclic diarylamines by protonation of the ring nitrogen.¹⁸ Hydroperoxides were determined in samples periodically withdrawn from each autoxidation using a coumarin-conjugated triarylphosphine, which undergoes a significant fluorescence enhancement upon oxidation with a hydroperoxide (Figure 3A).^{30,31} Since the rate constant for the oxidation of the phosphine by secondary hydroperoxides is known, the hydroperoxide concentration can be estimated from the initial rate (eq 4). The results are shown in Figure 3B and summarized in Figure 3C. The autoxidations were followed for the first 2% of the reaction (68 mM based on

hydroperoxide yield), since beyond ca. 3%, radical termination events predominate over chain propagation, leading to more ketones, alcohols, carboxylic acids, and esters (Figure 3B) in lieu of hydroperoxides.^{5,28} At this temperature, the hydroperoxide products decompose to generate initiating radicals resulting in a nonconstant rate of initiation, which precludes quantification of both the stoichiometry (n) and inhibition rate constants (k_{inh}) of the reaction of the diarylamines with peroxy radicals.⁵ Hence, we “quantified” the efficacy of the inhibition of the heterocyclic diarylamines relative to the models of the industry standard 4 and 5 by comparing the time required for conversion of the substrate to hydroperoxide to reach 2% ($\Delta t_{2\%}$, Figure 3C).

All compounds were effective inhibitors of *n*-hexadecane autoxidation and compared favorably to the two models of the industrial standard. It should be noted that these reactions were carried out in 95% *n*-hexadecane, where the (initial) rate of initiation is higher than in 99% *n*-hexadecane used in our previous studies¹⁸ due to residual unsaturation and other impurities in the sample. As such, compound 2, which exhibited a 12-fold greater inhibition time than 1 in 99% *n*-hexadecane, was found to inhibit only 6.4-fold longer in the present work. Most interestingly, the monomethylated compounds *p*-Me-2 and *o*-Me-2 and the neopentyl-substituted compound neopent-2 were significantly improved relative to 2, with inhibition times 18.2-, 12.8-, and 14.2-fold longer, respectively, than the models of the industrial standard. Furthermore, while the *t*-butylated and methylated compounds

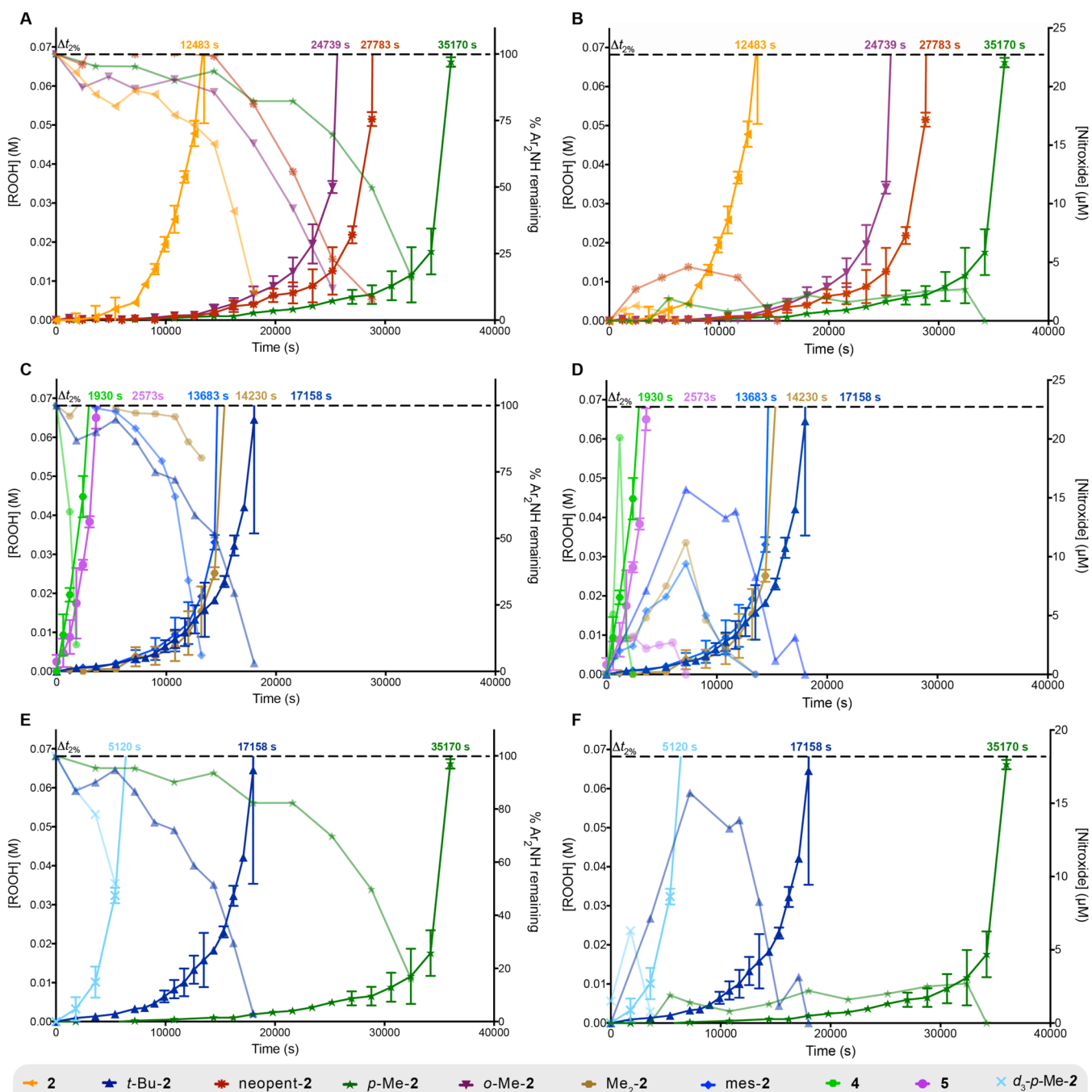


Figure 4. Loss of diarylamine (A, C, and E) and formation of nitroxide (B, D, and F) monitored over the course of the inhibited autoxidations of *n*-hexadecane at 160 °C shown in Figure 3.

t-Bu-2 and *p*-Me-2 were essentially indistinguishable at 37 and 100 °C, they differed considerably at 160 °C, with *t*-butyl substitution offering only a small increase in inhibition time over the unsubstituted 2. Indeed, *t*-Bu-2 was similarly effective to Me₂-2 and mes-2 at 160 °C, while being clearly superior at 37 and 100 °C. These results suggest that alkyl substitution can do more than simply prevent tautomerization of the peroxydiarylamyl adducts, and surprisingly, that nontertiary alkyl substitution is preferred for applications at higher temperatures.

Mechanistic Insights into the Benefit of Nontertiary Alkyl Substitution at Elevated Temperatures. To provide some insight into the origin of the superiority of nontertiary

alkyl substitution on the high-temperature reactivity of 2, we followed diarylamine consumption and nitroxide formation in autoxidations inhibited by the test compounds. Results are shown in Figure 4A–D. Expectedly, in each case, the depletion of the diarylamine coincides with an increase in hydroperoxide formation. However, the derivatives differ in the extent to which nitroxide accumulates during the inhibited period. Interestingly, the derivatives that give rise to a significant amount of nitroxide (i.e., *t*-Bu-2, Me₂-2, and mes-2, Figure 4B) are, in general, demonstrably less effective than those which do not (i.e., *p*-Me-2, *o*-Me-2, and neopent-2, Figure 4D).

To further probe the role of the methyl group on the enhanced activity of *p*-Me-2, we prepared a derivative wherein

each of the hydrogen atoms on the methyl group were replaced with deuterium atoms. Interestingly, while this substitution had essentially no impact on the inhibited period observed at either 37 or 100 °C (see the [Supporting Information](#)), a dramatic reduction in the inhibited period was observed at 160 °C ([Figure 4E,F](#)). Interestingly, this reduction was accompanied by an increase in nitroxide formation relative to the natural abundance isotopologue, fully consistent with the foregoing trend that nitroxide accumulation is greatest for poorer antioxidants under these conditions.

DISCUSSION

Alkylated diphenylamines are choice antioxidants for lubricants and other hydrocarbon products which experience elevated temperatures for sustained periods. Their advantage over phenols and other RTAs is believed to be due to their unique “catalytic” activity, generally ascribed to the Korcek cycle ([Figure 1C](#)). Progress through the Korcek cycle requires that the diarylaminy radical formed from initial H-atom transfer from the diarylamine to a peroxy radical be converted to a diarylnitroxide. Nitroxide formation competes with other reactions of the diarylaminy radical, such as homocoupling to yield tetrarylhydrazines and their isomerized counterparts, or addition of peroxy radicals to aryl ring carbons, which bear unpaired electron spin density (i.e., *ortho* and *para*).

As part of an effort to provide insight into the deleterious reactions that preclude progress through the Korcek cycle, we had previously computed that addition of a peroxy radical to the *para* carbon was preferred over peroxyamine formation (which leads to the nitroxide) by 1 kcal/mol. Although more thermodynamically favorable, this off-cycle reaction could, in principle, be overcome at elevated temperatures where ring addition is expected to be reversible while O–O cleavage to the nitroxide is not. In the current work, we expanded on these computations to find that the reverse reaction has another process with which it must compete: tautomerization. Tautomerization yields a peroxide with a much weaker O–O bond than the initial adduct (12 vs 41 kcal/mol) due to the formation of a highly stabilized aryloxy radical in place of an alkoxy radical. Although alkylation of the aryl ring makes peroxy radical addition more thermodynamically favorable, it prevents tautomerization at the alkylated position. At first glance, one may question whether it is reasonable to suggest that tautomerization is a likely pathway in a hydrocarbon substrate. As such, it is noteworthy that tautomerization of the product of the retro-carbonyl-ene reaction to yield the diphenylamine ([Figure 1D](#)) occurs readily in hexadecane (at least faster than the pericyclic reaction itself, which was studied between 90 and 150 °C).⁹ Thus, the omnipresence of alkyl substituents in commercial diphenylamine antioxidants serves not only to increase their solubility in hydrocarbon-based products and decrease their volatility at elevated temperatures, but also to suppress tautomerization, funneling diarylaminy radicals to nitroxides and promoting progress through the Korcek cycle.

Given this functional rationale for the incorporation of alkyl groups in commercial diphenylamines, we sought to explore the impact of alkyl substitution on the reactivity of diarylamine **2**, which we had previously characterized as significantly more potent than commercial alkylated diphenylamines. *Para*-alkylation of the phenyl ring in **2** leads to a modest (~1.5-fold) increase in its reactivity toward peroxy radicals at 37 °C regardless of the identity of the substituent (methyl, *t*-butyl,

and neopentyl), presumably due to a slight reduction of the N–H BDE by the modest electron-donating ability of the alkyl substituent (computed to be 0.5 kcal/mol for methyl). In contrast, the *ortho*-alkylated compounds were ~2-fold less reactive than **2**, presumably due to the steric hindrance imparted by the *ortho* methyl group(s) on the approach of the peroxy radical to the amine and, in the case of the mesityl derivative (*mes-2*), the fact that the diarylaminy radical cannot adopt a conformation allowing maximal delocalization of the unpaired electron across both aryl rings (see [Figure S2](#)).³² Radical-trapping stoichiometries were consistently $n \sim 2$ in the dioxane co-oxidations, as expected due to trapping of the initially formed diarylaminy radical with another peroxy radical to yield adducts that are largely stable at this temperature. Interestingly, stoichiometries derived from the inhibition times of the styrene co-oxidations were consistently higher (~5 for the *para*-alkylated derivatives and ~3.5 for the *ortho*-alkylated derivatives). This is reminiscent of recent observations we made for substituted phenoxazines, where values as large as $n \sim 12$ were found under these conditions.³³ This was attributed to the formation of a small amount of nitroxide from the amine, which is able to catalyze the cross-dismutation of alkylperoxy and hydroperoxy radicals formed in the autoxidation of unsaturated substrates.¹⁰ Indeed, when we monitored the styrene autoxidations inhibited by *t*-Bu-**2** and *p*-Me-**2** by electron paramagnetic resonance (EPR), we observed a low but steady concentration of nitroxide throughout the inhibited period (see [Figure S3](#)). Consistent with this mechanism, decreasing the rate of initiation (by 50%), which increases the lifetime of intermediate peroxy radicals, led to a modest increase in stoichiometry (~10%) as elimination of hydroperoxy radicals from styrene-derived peroxy radicals becomes increasingly competitive (see [Figure S3](#)).¹⁰

Catalysis of the cross-dismutation pathway was more evident in the data obtained in 1-hexadecene co-oxidations at 100 °C. *Para*-alkylation of the phenyl ring in **2** increased the stoichiometry from $n = 66$ to 75 (*t*-Bu-**2**), 70 (neopent-**2**), and 77 (*p*-Me-**2**), whereas *ortho*-alkylation generally lead to lower values (36–50), although still higher than the models of the industrial standard (31–34). We recently demonstrated that the high stoichiometric factors of **5** under these conditions were the result of nitroxide formation,¹⁰ and it follows that *para*-alkylation must increase the yield and/or persistence of the nitroxide while it is decreased by *ortho*-alkylation.

Again, when we monitored autoxidations inhibited by *t*-Bu-**2** and *p*-Me-**2** by EPR, we observed significant conversion of the amine to nitroxide (e.g., 1.2 μM for *t*-Bu-**2** and 0.8 μM for *p*-Me-**2**) and their concentrations tracked well with the inhibited period ([Figure S4](#)). Interestingly, although the maximum nitroxide concentration differed by 50% in the autoxidations inhibited by *t*-Bu-**2** and *p*-Me-**2**, reaction progress (as measured by PBD-BODIPY consumption) was virtually identical, suggesting that the formation of hydroperoxy radical from propagating 1-hexadecene-derived peroxy radicals is rate-limiting in the inhibitory activity of the compounds. Presumably, since *ortho* substitution should increase the persistence of the nitroxide derived from compound **2**, the lower activity of these derivatives must be due to a lower yield of nitroxide, consistent with their lower H-atom transfer reactivity (k_{inh}).

Interestingly, while at 37 and 100 °C, the alkylated derivatives of **2** were segregated into two distinct groups based upon the position of alkyl substitution (*para* vs *ortho*), at

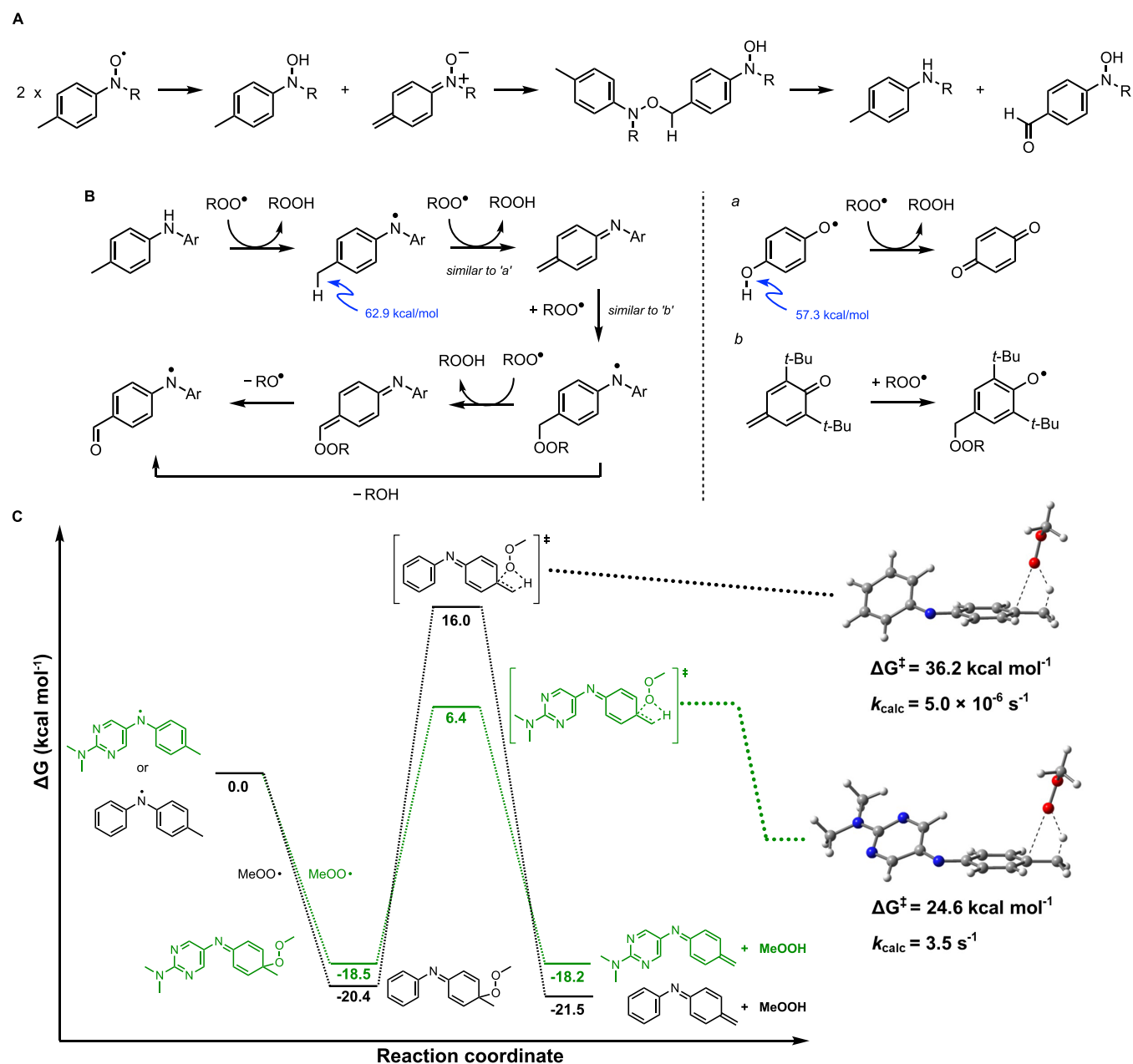


Figure 5. (A) Monoaryl nitroxide disproportionation, substitution, and elimination to yield amine and hydroxylamine, as reported by Forrester et al. (B) H-atom transfer from diarylaminy radicals featuring a *p*-methyl substituent is expected to lead to *p*-quinone-imine methide (similarly to semiquinone oxidation, a), which can undergo peroxyl radical addition (similarly to *p*-quinone methides, b), eventually leading to formylated diarylamines/diarylaminy radicals. (C) Relevant stationary points determined by CBS-QB3 for *syn* elimination of hydroperoxide from the peroxyl radical adduct of methylated diphenylaminyl and the diarylaminy radical derived from **2**. Calculated free-energy changes are given at 25 °C. Calculated barriers and associated rate constants determined from transition-state theory at 160 °C are also given.

160 °C, no such trend existed. For example, installation of a methyl group in the *ortho* and *para* positions of the phenyl ring of **2** extended the inhibition times by two- and threefold, respectively, while substitution with a *t*-butyl group led to a very modest increase of only ~33%. This is inconsistent with the expected persistence of the nitroxides derived therefrom. Indeed, when EPR was used to determine nitroxide formation in samples removed during these autoxidations, the increased inhibition times observed for the methylated derivatives were associated with significantly less nitroxide accumulation (e.g., 2 μM for *p*-Me-**2** vs 15 μM for *t*-Bu-**2**). Thus, paradoxically,

increased nitroxide formation appeared to be deleterious to the inhibitory activity of the diarylamine.

To probe any direct role of the benzylic position in the high-temperature RTA activity, we synthesized a deuterated analogue of *p*-Me-**2** and found a significant isotope effect on the inhibition time. Notably, *d*₃-*p*-Me-**2** had essentially indistinguishable activity from *p*-Me-**2** at 37 and 100 °C (Figure S5). This result indicates that H-atom transfer from the benzylic position is important to the improved catalytic radical-trapping activity of *p*-Me-**2** at elevated temperatures. Interestingly, this coincided with greater accumulation of

nitroxide, again suggesting that this is deleterious to the inhibitory activity of the diarylamine.

Forrester et al. has previously shown that nitroxides with benzylic positions undergo disproportionation to yield hydroxylamine and the corresponding quinone-imine methide *N*-oxide, which dimerize and fragment to produce hydroxylamine and regenerate the starting amine (Figure 5A).^{34–36}

While we considered this to be a tempting explanation, the low concentration of nitroxide that will exist—particularly when much of the amine has yet to be consumed—and the polar addition and elimination reactions by which the disproportionation are proposed to occur are expected to be unfavorable in *n*-hexadecane. Moreover, and perhaps most importantly, any hydroxylamine formed would be rapidly oxidized to nitroxide, which should have been easily visible to us by EPR, as it was to Forrester and Calder.^{34–36} Alternatively, we considered that H-atom transfer from the benzylic position of the diarylnitroxide may take place to a propagating peroxy radical, resulting in the formation of the same imino-quinone methide *N*-oxide. The strength of the benzylic C–H bond in the nitroxide is predicted by CBS-QB3 calculations to be a mere 73.4 kcal/mol, and therefore presumably the weakest C–H bond in the medium by a significant margin.³⁷ However, since the same imino-quinone methide *N*-oxide would be formed and it would be expected to undergo addition by either a peroxy radical or hydroperoxide, this should also lead to a similar accumulation of nitroxide.

Thus, we also considered the possibility that H-atom transfer from the benzylic position may occur from the diarylaminy radical (Figure 5B). Again, it seems less likely that this would take place as a disproportionation due to the low concentration of aminyl radicals, particularly when much of the amine has yet to be consumed, and instead by H-atom abstraction by a peroxy radical.³⁸ This reaction would compete directly with nitroxide formation via peroxy radical combination with the diarylaminy radical followed by O–O bond cleavage. Indeed, the benzylic C–H bond is even weaker in the diarylaminy radical (62.9 kcal/mol). This is reminiscent of the known reaction of a 1,4-semiquinone radical with a peroxy radical to yield a quinone, which has comparable thermodynamics.³⁹ Addition of a peroxy radical to the resultant quinone-imine methide is expected to follow and is reminiscent of the known addition of a peroxy radical to quinone methides, which we recently showed can be a decent chain-breaking reaction ($k \sim 10^4 \text{ M}^{-1} \text{ s}^{-1}$ at 37 °C).⁴⁰ Given the greater thermodynamic stability of the diarylaminy radical that results from addition to the *N*-aryl imino-quinone methide as compared to the phenoxyl radical resulting from addition to the quinone methide, the former should be an even better reaction than the latter. The resultant diarylaminy radical can be further oxidized to the *p*-formyl derivative, which could re-engage the Korcek cycle.

In contrast to the substantial difference between *t*-Bu-2 and *p*-Me-2, the substitution of the *t*-butyl groups of diphenylamine 4, a model of the typical structure of commercial alkylated diphenylamines, with methyl groups (5) led to a modest enhancement of activity (ca. 33%). Interestingly, the computed C–H BDE of the methyl substituent in the diarylaminy radical derived from 5 (63 kcal/mol) is even lower than that in the diarylaminy radical derived from *p*-Me-2 (66 kcal/mol), perhaps suggesting an H-atom transfer is not operative. As such, we wondered if, instead of a H-atom transfer, the reaction could proceed via an addition–elimination mechanism. Indeed, we were able to identify transition-state structures for the *syn*

elimination of methyl hydroperoxide from the methylperoxy radical adducts of *p*-Me-2 and 5, and the free-energy barrier to the former was ~ 12 kcal/mol lower than that to the latter (Figure 5C). It should be pointed out that these may represent upper bounds to the barriers of these reactions; H-atom abstraction from the diarylaminy radicals by the peroxy radical may be the preferred pathway, but this is impossible to accurately model with a single determinant wavefunction-based method. Regardless of the mechanism, this reaction is probably not relevant at lower temperatures, which is why all of the *para*-alkylated derivatives have essentially the same reactivity at 37 and 100 °C, but may underlie the dramatic differences at 160 °C. Overall, the addition–elimination sequence (or direct H-atom transfer) minimizes the concentration of the aminyl radical available for oxidation directly to the nitroxide or to undesirable off-cycle products. Moreover, it converts the initially formed diarylaminy radical to a less electron-rich diarylaminy radical that may more slowly undergo these deleterious side reactions. We are currently engaged in the design and execution of experiments that may provide further insight into this mechanistic proposal. These, and our efforts to deploy this simple substituent effect in the design and development of even more effective RTA systems, will be reported in due course.

■ EXPERIMENTAL SECTION

General. Reagents were purchased from commercial suppliers and used without further purification. The coumarin-conjugated triarylphosphine³¹ and PBD-BODIPY²² were prepared according to literature procedures. Compounds 4⁴¹ and 5⁴² were prepared using the general Buchwald–Hartwig cross-coupling methodology described below. All reactions which required heating were carried out in a thermostatted oil bath. Column chromatography was carried out using flash silica gel (40–63 μm , 230–400 mesh). ¹H and ¹³C NMR spectra were recorded on a Bruker AVANCE spectrometer at 400 and 100 MHz, respectively, unless specified otherwise. High-resolution mass spectra were obtained on a Kratos Concept Tandem mass spectrometer using a magnetic sector mass analyzer. Calculations were carried out using the CBS-QB3⁴³ complete basis set method as implemented in the Gaussian 16 suite of programs.⁴⁴

General Method for the Preparation of 5-Bromo-*N,N*-dialkylaminopyrimidines. To a solution of 5-bromo-2-aminopyrimidine (1.0 mmol, 1.0 equiv) in dry tetrahydrofuran (THF; 2 mL, 0.5 M) at 50 °C, NaH (2.2 mmol) was added slowly and the mixture was stirred until H₂ evolution ceased (~ 20 min). Either *n*-hexylbromide (2.1 mmol, 2.1 equiv) or *n*-octylbromide (2.1 mmol, 2.1 equiv) was then added and the reaction was refluxed overnight. The reaction was cooled, quenched with MeOH, and extracted with Et₂O. The combined organics were washed with brine and dried over MgSO₄. The solvent was evaporated and the oil obtained was passed through a plug of silica (20% Et₂O/hexanes) to obtain the product in analytical purity. Characterization data were in accordance with the literature.^{18,45}

General Procedure for Buchwald–Hartwig Cross-Couplings. To a Schlenk flask, Pd₂dba₃ (0.01 mmol, 10 mol %) and BippyPhos (Pd/L = 1:4, 0.04 mmol) were added. The flask was evacuated and backfilled with argon before *tert*-amylalcohol (1 mL, 1 M) was added, followed by KOH (1.5 mmol, 1.5 equiv) and H₂O (0.1 mL, 1.0% v/v), and the solution was stirred for 20 min. After 20 min, aryl bromide (1.0 mmol, 1 equiv) and arylamine (1.2 mmol, 1.2 equiv) were added, and the reaction was heated to 110 °C. Once the reaction was judged complete by thin-layer chromatography (TLC) analysis (~ 36 h), the solvent was removed under reduced pressure and the residue loaded on a silica gel flash column. Column chromatography (Et₂O/hexanes eluent with 1–3% Et₃N) afforded the product in analytical purity.

***N*²,*N*²-Diocetyl-*N*⁵-phenylpyrimidine-2,5-diamine (2).** Yield: 4.6 g, 89%. Yellow oil. Mobile phase for purification: 40% Et₂O/hexanes with 3% Et₃N. ¹H NMR (400 MHz, DMSO-*d*₆) δ 8.19 (s, 2H), 7.52 (s, 1H), 7.11 (dd, *J* = 8.5, 7.2 Hz, 2H), 6.70 (dt, *J* = 7.7, 1.1 Hz, 2H), 6.68–6.63 (m, 1H), 3.54–3.43 (m, 4H), 1.54 (t, *J* = 7.2 Hz, 4H), 1.34–1.15 (m, 21H), 0.89–0.81 (m, 6H). ¹³C{H} NMR (101 MHz, DMSO-*d*₆) δ 158.4, 153.6, 147.0, 129.6, 126.4, 118.2, 113.7, 47.7, 31.6, 29.3, 29.1, 27.7, 26.8, 22.5, 14.4. HRMS (EI) *m/z*: [M]⁺ calcd for C₂₆H₄₂N₄ 410.3409; found 410.3390.

***N*⁵-(4-(*tert*-Butyl)phenyl)-*N*²,*N*²-diocetylpyrimidine-2,5-diamine (*t*-Bu-2).** 5.4 g, Yield: 92%. Brown oil. Mobile phase for purification: 20% Et₂O/hexanes with 1% Et₃N. ¹H NMR (400 MHz, DMSO-*d*₆) δ 8.17 (s, 2H), 7.38 (s, 1H), 7.18–7.09 (m, 2H), 6.65 (d, *J* = 8.7 Hz, 2H), 3.53–3.42 (m, 4H), 1.54 (t, *J* = 7.2 Hz, 4H), 1.35–1.22 (m, 20H), 1.21 (s, 9H), 0.89–0.79 (m, 6H). ¹³C{H} NMR (101 MHz, DMSO-*d*₆) δ 153.1, 126.1, 113.6, 47.6, 34.0, 31.8, 31.7, 29.3, 29.1, 27.8, 26.9, 22.5, 14.4. HRMS (EI) *m/z*: [M]⁺ calcd for C₃₀H₅₀N₄ 466.4035; found, 466.4013.

***N*²,*N*²-Dibutyl-*N*⁵-(4-*neopentyl*phenyl)pyrimidine-2,5-diamine (*neopent*-2).** 1.8 g, Yield: 91%. Yellow oil. Mobile phase for purification: 20% Et₂O/hexanes with 1% Et₃N. ¹H NMR (400 MHz, DMSO-*d*₆) δ 8.19 (d, *J* = 0.7 Hz, 2H), 7.40 (s, 1H), 6.88 (d, *J* = 8.4 Hz, 2H), 6.64 (d, *J* = 8.3 Hz, 2H), 3.57–3.42 (m, 4H), 2.32 (s, 2H), 1.59–1.48 (m, 4H), 1.29 (h, *J* = 7.4 Hz, 4H), 0.91 (t, *J* = 7.3 Hz, 7H), 0.83 (s, 9H). ¹³C{H} NMR (101 MHz, DMSO-*d*₆) δ 158.3, 153.1, 144.9, 131.3, 128.9, 127.0, 113.4, 49.1, 47.4, 31.8, 30.0, 29.5, 20.1, 14.3. HRMS (EI) *m/z*: [M]⁺ calcd for C₂₃H₃₆N₄ 368.2940; found, 368.2918.

***N*²,*N*²-Diocetyl-*N*⁵-(*p*-tolyl)pyrimidine-2,5-diamine (*p*-Me-2).** Yield: 4.8 g, 88%. Clear oil. Mobile phase for purification: 30% Et₂O/hexanes with 2% Et₃N. ¹H NMR (400 MHz, DMSO-*d*₆) δ 8.16 (s, 2H), 7.36 (s, 1H), 6.93 (d, *J* = 8.1 Hz, 2H), 6.64 (d, *J* = 8.4 Hz, 2H), 3.48 (dd, *J* = 8.7, 6.3 Hz, 4H), 2.16 (s, 3H), 1.62–1.46 (m, 4H), 1.36–1.15 (m, 21H), 0.88–0.78 (m, 6H). ¹³C{H} NMR (101 MHz, DMSO-*d*₆) δ 152.8, 144.4, 130.0, 126.8, 114.1, 47.7, 31.7, 29.3, 29.1, 27.8, 26.9, 22.5, 20.5, 14.4. HRMS (EI) *m/z*: [M]⁺ calcd for C₂₇H₄₄N₄ 424.3566; found, 424.3577.

***N*²,*N*²-Diocetyl-*N*⁵-(*o*-tolyl)pyrimidine-2,5-diamine (*o*-Me-2).** Yield: 1.0 g, 96%. Clear oil. Mobile phase for purification: 20% Et₂O/hexanes with 1% Et₃N. ¹H NMR (400 MHz, DMSO-*d*₆) δ 8.15 (s, 2H), 7.11–7.02 (m, 1H), 6.95 (t, *J* = 7.7 Hz, 1H), 6.71 (s, 1H), 6.64 (td, *J* = 7.5, 1.1 Hz, 1H), 6.54 (d, *J* = 8.2 Hz, 1H), 3.49 (t, *J* = 7.5 Hz, 4H), 2.20 (s, 3H), 1.54 (p, *J* = 7.5, 7.0 Hz, 4H), 1.30–1.20 (m, 20H), 0.88–0.82 (m, 6H). ¹³C{H} NMR (101 MHz, DMSO-*d*₆) δ 158.4, 154.1, 145.2, 130.9, 127.0, 126.9, 118.7, 112.5, 47.6, 31.6, 29.3, 29.1, 27.7, 26.8, 22.5, 18.2, 14.4. HRMS (EI) *m/z*: [M]⁺ calcd for C₂₇H₄₄N₄ 424.3566; found, 424.3569.

***N*⁵-(2,4-Dimethylphenyl)-*N*²,*N*²-dihexylpyrimidine-2,5-diamine (*Me*₂-2).** Yield: 0.9 g, 82% Brown oil. Mobile phase for purification: 20% Et₂O/hexanes with 1% Et₃N. ¹H NMR (400 MHz, DMSO-*d*₆) δ 8.11 (s, 2H), 6.89 (d, *J* = 2.0 Hz, 1H), 6.82–6.74 (m, 1H), 6.59 (s, 1H), 6.51 (d, *J* = 8.1 Hz, 1H), 3.48 (dd, *J* = 8.5, 6.4 Hz, 4H), 2.16 (d, *J* = 3.4 Hz, 6H), 1.55 (d, *J* = 7.8 Hz, 4H), 1.33–1.19 (m, 12H), 0.91–0.78 (m, 6H). ¹³C{H} NMR (101 MHz, DMSO-*d*₆) δ 158.2, 153.0, 142.5, 131.7, 127.7, 127.6, 127.3, 124.9, 113.6, 47.6, 31.6, 27.8, 26.6, 22.5, 20.5, 18.2, 14.3. HRMS (EI) *m/z*: [M]⁺ calcd for C₂₄H₃₈N₄ 382.3096; found, 382.3073.

***N*²,*N*²-Dihexyl-*N*⁵-mesitylpyrimidine-2,5-diamine (*mes*-2).** Yield: 0.8 g, 72% Brown oil. Mobile phase for purification: 20% Et₂O/hexanes with 1% Et₃N. ¹H NMR (400 MHz, DMSO-*d*₆) δ 7.61 (s, 2H), 6.89 (s, 2H), 6.62 (s, 1H), 3.44–3.35 (m, 4H), 2.22 (s, 3H), 2.08 (s, 7H), 1.53–1.40 (m, 4H), 1.24 (s, 13H), 0.84 (q, *J* = 5.0, 3.5 Hz, 6H). ¹³C{H} NMR (101 MHz, DMSO-*d*₆) δ 156.4, 144.2, 136.6, 134.4, 133.9, 132.1, 129.5, 47.6, 31.6, 27.9, 26.6, 22.5, 20.9, 18.4, 14.3. HRMS (EI) *m/z*: [M]⁺ calcd for C₂₅H₄₀N₄ 396.3253; found, 396.3270.

***N*²,*N*²-Diocetyl-*N*⁵-(4-(methyl-*d*₃)phenyl)pyrimidine-2,5-diamine (*d*₃-*p*-Me-2).** Yield: 0.2 g, 34% Brown oil. Mobile phase for purification: 30% Et₂O/hexanes with 2% Et₃N. ¹H NMR (400 MHz, DMSO-*d*₆) δ 8.17 (s, 2H), 7.37 (s, 1H), 6.94 (d, *J* = 8.4 Hz,

2H), 6.65 (d, *J* = 8.5 Hz, 2H), 3.49 (t, *J* = 7.4 Hz, 4H), 1.58–1.48 (m, 4H), 1.27–1.45 (m, 20H), 0.87 (t, *J* = 6.72 Hz, 6H). ¹³C{H} NMR (101 MHz, DMSO-*d*₆) δ 157.8, 152.4, 144.0, 129.6, 126.6, 126.3, 113.7, 47.2, 31.2, 28.8, 28.7, 27.3, 26.4, 22.1, 13.9. HRMS (EI) *m/z*: [M]⁺ calcd for C₂₇H₄₁D₃N₄ 427.3754; found, 427.3779.

Inhibited Autoxidation of 1,4-Dioxane at 37 °C. A 3.5 mL quartz cuvette was loaded with unstabilized 1,4-dioxane (0.625 mL) along with PhCl (1.805 mL). The cuvette was then preheated to 37 °C for approximately 5 min. The cuvette was blanked and 12.5 μL of 2 mM PBD-BODIPY in 1,2,4-trichlorobenzene was added followed by 50 μL of 0.3 M AIBN in chlorobenzene followed by thorough mixing. After 10 min, an aliquot of the antioxidant stock solution (1 mM) in chlorobenzene was added, and the loss of absorbance at 587 nm was followed. The inhibition rate constant (*k*_{inh}) and stoichiometry (*n*) were determined for each experiment according to the equations in Figure 2. Rate constants and standard derivations are derived from three independent experiments.

Inhibited Autoxidation of Styrene at 37 °C. Styrene was washed thrice with 1 M aqueous NaOH, dried over MgSO₄, filtered, distilled under vacuum, and purified by percolating through silica and then basic alumina. To a cuvette containing 1.25 mL of styrene, 1.18 mL of chlorobenzene was added and the solution equilibrated for 5 min at 37 °C. The cuvette was blanked and 12.5 μL of 2 mM PBD-BODIPY in 1,2,4-trichlorobenzene was added followed by 50 μL of 0.3 M AIBN in chlorobenzene and the solution was thoroughly mixed. After 40 min, an aliquot of an RTA stock solution (1 mM) in chlorobenzene was added and the loss of absorbance at 591 nm was followed. The inhibition rate constant (*k*_{inh}) and stoichiometry (*n*) were determined for each experiment according to equations in Figure 2. Kinetic data are given as averages of three independent measurements.

Inhibited Autoxidation of 1-Hexadecene at 100 °C. 1-Hexadecene was purified prior to autoxidations by percolating through a column of silica and basic alumina. To a cuvette containing 0.44 mL of PhCl, 2.00 mL of 1-hexadecene was added. The cuvette was preheated to 100 °C in a UV-vis spectrophotometer and allowed to equilibrate for 10 min. The cuvette was blanked and PBD-BODIPY (12.5 μL of a 2.00 mM stock solution in 1,2,4-trichlorobenzene) and 50 μL of a 50 mM stock solution of dicumyl peroxide in chlorobenzene were added. The solution was thoroughly mixed prior to monitoring the uninhibited co-autoxidation via the disappearance of PBD-BODIPY. After 10 min, an aliquot of an antioxidant stock solution in chlorobenzene was added and the loss of absorbance at 587 nm was followed. The inhibition rate constant (*k*_{inh}) and stoichiometry (*n*) were determined for each experiment according to the equations in Figure 2. Rate constants and standard derivations are derived from three independent experiments.

Inhibited Autoxidations of *n*-Hexadecane at 160 °C. Hexadecane (10 mL) was added to test tubes in a 24-place stirred-flow reactor, thoroughly degassed with argon, and then heated to 160 °C. Once the temperature stabilized, 300 μM inhibitors and 2 mM Primene base were added to the test tubes, and the flow of argon was replaced with O₂. An aliquot (0.1 mL) was withdrawn at regular intervals and allowed to cool to room temperature for analysis.

Quantification of Hydroperoxides. A small volume (5 μL) of each sample was loaded into the wells of a 96-well microplate and diluted with 2-propanol and methanol (1:4:215 mL) using the automated reagent dispenser of the microplate reader. Next, 30 μL of a solution containing the fluorogenic coumarin phosphine dye (100 mM) in acetonitrile was added to each well again using the automated reagent dispenser. The plate, incubated at 37 °C, was stirred for 30 s, and after a 5 s delay, the fluorescence of each well was measured every second for 60 s (excitation = 340 nm and emission = 425 nm). The concentration of hydroperoxide in each well was determined from the rate of phosphine oxidation using the rate constant for the reaction of the dye with secondary hydroperoxides (*k* = 5.1 M⁻¹ s⁻¹), assuming pseudo-first-order kinetics.

Quantification of Diarylamine Consumption. A small volume (5 μL) of each sample was loaded into the wells of a 96-well microplate and diluted with 2-propanol and methanol (1:4:215 mL)

using the automated reagent dispenser of the microplate reader. Next, fluorescence spectra of each diarylamine were recorded between 300 and 700 nm by exciting at 360 nm. The percentage of diarylamine content was determined by setting $t = 0$ as 100% diarylamine (300 μM).

Quantification of Nitroxides by EPR. Electron paramagnetic resonance (EPR) spectra were recorded on a Bruker EMXplus (X-band) spectrometer equipped with an ER 4119HS cavity. Samples (100 μL) obtained from hexadecane, styrene, or 1,4-dioxane autoxidations were loaded in a thin glass capillary and placed in an EPR tube. The radical concentration was determined at ambient temperatures using the quantitative EPR package of the Bruker Xenon software.

■ ASSOCIATED CONTENT

SI Supporting Information

The Supporting Information is available free of charge at <https://pubs.acs.org/doi/10.1021/acs.joc.1c00365>.

Additional computational and experimental procedures and results, compound characterization data, and Cartesian coordinates of computed structures (PDF)

■ AUTHOR INFORMATION

Corresponding Author

Derek A. Pratt – Department of Chemistry and Biomolecular Sciences, University of Ottawa, Ottawa, Ontario, Canada K1N 6N5; orcid.org/0000-0002-7305-745X; Email: dpratt@uottawa.ca

Authors

Ron Shah – Department of Chemistry and Biomolecular Sciences, University of Ottawa, Ottawa, Ontario, Canada K1N 6N5

Jia-Fei Poon – Department of Chemistry and Biomolecular Sciences, University of Ottawa, Ottawa, Ontario, Canada K1N 6N5

Evan A. Haidasz – Department of Chemistry and Biomolecular Sciences, University of Ottawa, Ottawa, Ontario, Canada K1N 6N5

Complete contact information is available at: <https://pubs.acs.org/doi/10.1021/acs.joc.1c00365>

Notes

The authors declare no competing financial interest.

■ ACKNOWLEDGMENTS

This work was supported by grants from the Natural Sciences and Engineering Research Council (NSERC) of Canada and the Canada Foundation for Innovation. R.S. and E.A.H. acknowledge NSERC and the Government of Ontario for their support via postgraduate scholarships.

■ REFERENCES

- (1) (a) Bolland, J. L. Kinetics of Olefin Oxidation. *Q. Rev., Chem. Soc.* **1949**, *3*, 1–21. (b) Bateman, L. Olefin Oxidation. *Q. Rev., Chem. Soc.* **1954**, *8*, 147–167.
- (2) (a) Yin, H.; Xu, L.; Porter, N. A. Free Radical Lipid Peroxidation: Mechanisms and Analysis. *Chem. Rev.* **2011**, *111*, 5944–5972. (b) Conrad, M.; Pratt, D. A. The Chemical Basis of Ferroptosis. *Nat. Chem. Biol.* **2019**, *15*, 1137–1147.
- (3) Ingold, K. U. Inhibition of the Autoxidation of Organic Substances in the Liquid Phase. *Chem. Rev.* **1961**, *61*, 563–589.

(4) Ingold, K. U.; Pratt, D. A. Advances in Radical-Trapping Antioxidant Chemistry in the 21st Century: A Kinetics and Mechanisms Perspective. *Chem. Rev.* **2014**, *114*, 9022–9046.

(5) Jensen, R. K.; Korcek, S.; Zinbo, M.; Johnson, M. D. Initiation in Hydrocarbon Autoxidation at Elevated Temperatures. *Int. J. Chem. Kinet.* **1990**, *22*, 1095–1107.

(6) Brownlie, I. T.; Ingold, K. U. The Inhibited Autoxidation Of Styrene: Part V. The Kinetics And Deuterium Isotope Effect For Inhibition By Diphenylamine, Phenyl-A-Naphthylamine, And Phenyl-B-Naphthylamine. *Can. J. Chem.* **1966**, *44*, 861–868.

(7) Jensen, R. K.; Korcek, S.; Zinbo, M.; Gerlock, J. L. Regeneration of Amine in Catalytic Inhibition of Oxidation. *J. Org. Chem.* **1995**, *60*, 5396–5400.

(8) Bolsman, T. A. B. M.; Blok, A. P.; Frijns, J. H. G. Mechanism of the Catalytic Inhibition of Hydrocarbon Autoxidation by Secondary Amines and Nitroxides. *Recl. Trav. Chim. Pays-Bas* **1978**, *97*, 310–312.

(9) Haidasz, E. A.; Shah, R.; Pratt, D. A. The Catalytic Mechanism of Diarylamine Radical-Trapping Antioxidants. *J. Am. Chem. Soc.* **2014**, *136*, 16643–16650.

(10) Harrison, K. A.; Haidasz, E. A.; Griesser, M.; Pratt, D. A. Inhibition of Hydrocarbon Autoxidation by Nitroxide-Catalyzed Cross-Dismutation of Hydroperoxyl and Alkylperoxyl Radicals. *Chem. Sci.* **2018**, *9*, 6068–6079.

(11) Baschieri, A.; Valgimigli, L.; Gabbanini, S.; Dilabio, G. A.; Romero-Montalvo, E.; Amorati, R. Extremely Fast Hydrogen Atom Transfer between Nitroxides and HOO· Radicals and Implication for Catalytic Coantioxidant Systems. *J. Am. Chem. Soc.* **2018**, *140*, 10354–10362.

(12) This was demonstrated by Baschieri et al.¹¹ at 30 °C, where HOO· is a chain-propagating radical in autoxidations of 1,3-cyclohexadiene. Harrison et al.¹⁰ show that HOO· is a by-product of unsaturated hydrocarbon autoxidation, in general.

(13) Pratt, D. A.; DiLabio, G. A.; Valgimigli, L.; Pedulli, G. F.; Ingold, K. U. Substituent Effects on the Bond Dissociation Enthalpies of Aromatic Amines. *J. Am. Chem. Soc.* **2002**, *124*, 11085–11092.

(14) Hanthorn, J. J.; Valgimigli, L.; Pratt, D. A. Incorporation of Ring Nitrogens into Diphenylamine Antioxidants: Striking a Balance between Reactivity and Stability. *J. Am. Chem. Soc.* **2012**, *134*, 8306–8309.

(15) Hanthorn, J. J.; Valgimigli, L.; Pratt, D. A. Preparation of Highly Reactive Pyridine- and Pyrimidine-Containing Diarylamine Antioxidants. *J. Org. Chem.* **2012**, *77*, 6908–6916.

(16) Hanthorn, J. J.; Amorati, R.; Valgimigli, L.; Pratt, D. A. The Reactivity of Air-Stable Pyridine- and Pyrimidine-Containing Diarylamine Antioxidants. *J. Org. Chem.* **2012**, *77*, 6895–6907.

(17) In our previous work we compare the reactivity of the heterocyclic diarylamines to bis(4-octylphenyl)amine **1**. However, since *tert*-alkylated diphenylamines are invariably used in relevant applications, compound **3** is a better model with which to compare.

(18) Shah, R.; Haidasz, E. A.; Valgimigli, L.; Pratt, D. A. Unprecedented Inhibition of Hydrocarbon Autoxidation by Diarylamine Radical-Trapping Antioxidants. *J. Am. Chem. Soc.* **2015**, *137*, 2440–2443.

(19) Bennett, J. E.; Brunton, G.; Forrester, A. R.; Fullerton, J. D. Reactivity and Structure of N-Phenylnaphth-1-ylamines and Related Compounds. Part 1. Reactions with Alkylperoxyl Radicals. *J. Chem. Soc., Perkin Trans. 2* **1983**, *9*, 1477–1480.

(20) Cardellini, L.; Carloni, P.; Greci, L.; Stipa, P.; Fautitano, A. Homolytic Substitutions in Indolinone Nitroxide Radicals. Part 5. Reaction with Tert-Butylperoxy Radicals. *Gazz. Chim. Ital.* **1989**, *119* (12), 621–625.

(21) Ingold, K. U.; Howard, J. A. Absolute Rate Constants for Hydrocarbon Autoxidation. XVII. The Oxidation of Some Cyclic Ethers. *Can. J. Chem.* **1969**, *47*, 3809–3815.

(22) Haidasz, E. A.; Van Kessel, A. T. M.; Pratt, D. A. A Continuous Visible Light Spectrophotometric Approach To Accurately Determine the Reactivity of Radical-Trapping Antioxidants. *J. Org. Chem.* **2016**, *81*, 737–744.

(23) Snelgrove, D. W.; Luszyk, J.; Banks, J. T.; Mulder, P.; Ingold, K. U. Kinetic Solvent Effects on Hydrogen-Atom Abstractions: Reliable, Quantitative Predictions via a Single Empirical Equation. *J. Am. Chem. Soc.* **2001**, *123*, 469–477.

(24) Litwinienko, G.; Ingold, K. U. Solvent Effects on the Rates and Mechanisms of Reaction of Phenols with Free Radicals. *Acc. Chem. Res.* **2007**, *40*, 222–230.

(25) Abraham, M. H.; Grellier, P. L.; Prior, D. V.; Duce, P. P.; Morris, J. J.; Taylor, P. J. Hydrogen Bonding. Part 7. A Scale of Solute Hydrogen-Bond Acidity Based on Log K Values for Complexation in Tetrachloromethane. *J. Chem. Soc., Perkin Trans. 2* **1989**, 699–711.

(26) Abraham, M. H.; Grellier, P. L.; Prior, D. V.; Morris, J. J.; Taylor, P. J. Hydrogen Bonding. Part 10. A Scale of Solute Hydrogen-Bond Basicity Using Log K Values for Complexation in Tetrachloromethane. *J. Chem. Soc., Perkin Trans. 2* **1990**, *4*, 521.

(27) Abraham, M. H.; Abraham, R. J.; Byrne, J.; Griffiths, L. NMR Method for the Determination of Solute Hydrogen Bond Acidity. *J. Org. Chem.* **2006**, *71*, 3389–3394.

(28) Jensen, R. K.; Korcek, S.; Mahoney, L. R.; Zinbo, M. Liquid-Phase Autoxidation of Organic Compounds at Elevated Temperatures. 1. The Stirred Flow Reactor Technique and Analysis of Primary Products from n-Hexadecane Autoxidation at 120–180-Degree.C. *J. Am. Chem. Soc.* **1979**, *101*, 7574–7584.

(29) Igarashi, J.; Jensen, R. K.; Luszyk, J.; Korcek, S.; Ingold, K. U. Autoxidation of Alkyl-naphthalenes. 2. Inhibition of the Autoxidation of n-Hexadecane at 160 °C. *J. Am. Chem. Soc.* **1992**, *114*, 7727–7736.

(30) Shah, R.; Pratt, D. A. Determination of Key Hydrocarbon Autoxidation Products By Fluorescence. *J. Org. Chem.* **2016**, *81*, 6649–6656.

(31) Hanthorn, J. J.; Haidasz, E.; Gebhardt, P.; Pratt, D. A. A Versatile Fluorescence Approach to Kinetic Studies of Hydrocarbon Autoxidations and Their Inhibition by Radical-Trapping Antioxidants. *Chem. Commun.* **2012**, *48*, 10141–10143.

(32) Levitskiy, O. A.; Sentyurin, V. V.; Magdesieva, T. V. Twisting of Diarylnitroxides: An Efficient Tool for Redox Tuning. *Electrochim. Acta* **2018**, *260*, 459–467.

(33) Farmer, L. A.; Haidasz, E. A.; Griesser, M.; Pratt, D. A. Phenoxazine: A Privileged Scaffold for Radical-Trapping Antioxidants. *J. Org. Chem.* **2017**, *82*, 10523–10536.

(34) Forrester, A. R.; Hepburn, S. P. Nitroxide Radicals. Part VIII. Stability of Ortho-Alkyl-Substituted Phenyl t-Butyl Nitroxides. *J. Chem. Soc.* **1969**, *9*, 1277–1280.

(35) Calder, A.; Forrester, A. R. The Stability of Aryl-t-Butylnitroxides. *Chem. Commun.* **1967**, *14*, 682–684.

(36) Calder, A.; Forrester, A. R. Nitroxide Radicals. Part VI. Stability of Meta- and Para-Alkyl Substituted Phenyl-t-Butylnitroxides. *J. Chem. Soc. C* **1969**, *No. 10*, 1459–1464.

(37) Unfortunately, the necessity to carry out a prohibitively costly multi-reference configuration interaction calculation to accurately predict the barrier for H-atom transfer from the diarylnitroxide to a peroxy radical precludes any insight on the associated kinetics of this process.

(38) It should be pointed out that CBS-QB3 calculations reveal that while the disproportionation of the nitroxides derived from *p*-Me-2 and *p*-methyl diphenylamine is uphill, with $\Delta G = 9.9$ and 4.0 kcal/mol, respectively, disproportionation of the corresponding diphenylaminyl radicals is downhill, with $\Delta G = -14.5$ and -21.0 kcal/mol, respectively.

(39) Valgimigli, L.; Amorati, R.; Fumo, M. G.; DiLabio, G. A.; Pedulli, G. F.; Ingold, K. U.; Pratt, D. A. The Unusual Reaction of Semiquinone Radicals with Molecular Oxygen. *J. Org. Chem.* **2008**, *73*, 1830–1841.

(40) Raycroft, M. A. R.; Chauvin, J. P. R.; Galliher, M. S.; Romero, K. J.; Stephenson, C. R. J.; Pratt, D. A. Quinone Methide Dimers Lacking Labile Hydrogen Atoms Are Surprisingly Excellent Radical-Trapping Antioxidants. *Chem. Sci.* **2020**, *11*, 5676–5689.

(41) Zhao, H.; Tanjutco, C.; Thayumanavan, S. Design and Synthesis of Stable Triarylamines for Hole-Transport Applications. *Tetrahedron Lett.* **2001**, *42*, 4421–4424.

(42) Green, R. A.; Hartwig, J. F. Palladium-Catalyzed Amination of Aryl Chlorides and Bromides with Ammonium Salts. *Org. Lett.* **2014**, *16*, 4388–4391.

(43) Montgomery, J. A.; Frisch, M. J.; Ochterski, J. W.; Petersson, G. A. A Complete Basis Set Model Chemistry. VI. Use of Density Functional Geometries and Frequencies. *J. Chem. Phys.* **1999**, *110*, 2822–2827.

(44) Frisch, M. J.; Trucks, G. W.; Schlegel, H. B.; Scuseria, G. E.; Robb, M. A.; Cheeseman, J. R.; Scalmani, G.; Barone, V.; Petersson, G. A.; Nakatsuji, H.; Li, X.; Caricato, M.; Marenich, A. V.; Bloino, J.; Janesko, B. G.; Gomperts, R.; Mennucci, B.; Hratchian, H. P.; Ortiz, J. V.; Izmaylov, A. F.; Sonnenberg, J. L.; Williams, Ding, F.; Lipparini, F.; Egidi, F.; Goings, J.; Peng, B.; Petrone, A.; Henderson, T.; Ranasinghe, D.; Zakrzewski, V. G.; Gao, J.; Rega, N.; Zheng, G.; Liang, W.; Hada, M.; Ehara, M.; Toyota, K.; Fukuda, R.; Hasegawa, J.; Ishida, M.; Nakajima, T.; Honda, Y.; Kitao, O.; Nakai, H.; Vreven, T.; Throssell, K.; Montgomery, J. A., Jr.; Peralta, J. E.; Ogliaro, F.; Bearpark, M. J.; Heyd, J. J.; Brothers, E. N.; Kudin, K. N.; Staroverov, V. N.; Keith, T. A.; Kobayashi, R.; Normand, J.; Raghavachari, K.; Rendell, A. P.; Burant, J. C.; Iyengar, S. S.; Tomasi, J.; Cossi, M.; Millam, J. M.; Klene, M.; Adamo, C.; Cammi, R.; Ochterski, J. W.; Martin, R. L.; Morokuma, K.; Farkas, O.; Foresman, J. B.; Fox, D. J. *Gaussian 16*, revision A.03; Gaussian, Inc.: Wallingford, CT, 2016.

(45) Shah, R.; Margison, K.; Pratt, D. A. The Potency of Diarylamine Radical-Trapping Antioxidants as Inhibitors of Ferrop-tosis Underscores the Role of Autoxidation in the Mechanism of Cell Death. *ACS Chem. Biol.* **2017**, *12*, 2538–2545.